

## Numerical analysis of three-dimensional Bingham plastic flow

C.R. Beverly and R.I. Tanner

*Department of Mechanical Engineering, The University of Sydney, NSW 2006 (Australia)*

(Received September 19, 1991)

### Abstract

The present paper considers the problem of predicting motionless regions and true plug (constant velocity areas where the stress is below the yield stress) regimes for fully three-dimensional Bingham plastic flows. Numerical solutions are obtained using a finite-element biviscosity formulation. Comparisons are drawn to alternative numerical approximations and a review of common finite elements is made with a view to finding accurate, stable and economical schemes. A number of elements are compared and we conclude that some of the Fortin elements are most useful on the grounds of computational overhead and solution accuracy. These are used to investigate axial flows of a Bingham body in an annulus. Finally, we show that the numerical solutions of the axial flow of a Bingham plastic in a narrow eccentric annulus show good agreement with observations and theoretical predictions.

*Keywords:* Bingham plastic; biviscosity formulation; eccentric annulus; three-dimensional finite elements

---

### 1. Introduction

An important idealised class of non-Newtonian materials possesses a yield stress which must be exceeded before significant deformation can occur. Such materials can sustain an applied stress at rest and include greases, slurries and doughs. A variety of non-Newtonian models have been

---

*Correspondence to:* R.I. Tanner, Department of Mechanical Engineering, The University of Sydney, NSW 2006, Australia.

proposed to predict the rheological behaviour of such materials on the basis of empiricism and experimental observation; see for example Bird et al. [1]. A most useful and popular model, namely the Bingham body, is described below.

The Bingham model is one of the simplest models that describes materials with yield stress,  $\tau_y$ . It is characterised by a flow curve (shear stress ( $\tau$ ) as a function of shear rate ( $\dot{\gamma}$ )) which is a straight line having an intercept  $\tau_y$  on the shear stress axis, and it is this yield stress that must be exceeded before commencement of flow is possible, the rate of deformation then being proportional to the excess of the stress over the yield condition. Typically the fluid response after yield is taken to be linear in the deformation rate so that the material may be viewed as a complicated generalised Newtonian fluid. Within the unyielded region the material must flow as a rigid body which constrains the rate-of-deformation tensor to be identically zero. In general terms the system behaves as a Newtonian fluid under the influence of a shear stress equivalent to  $\tau - \tau_y$ ; when the shear stress  $\tau$  falls below  $\tau_y$  a solid structure is formed.

The general form of the Bingham model is presented in Refs. 1 and 2 and is summarised as

$$\tau_{ij} = 2 \left( \frac{\tau_y}{\dot{\gamma}} + \eta_0 \right) d_{ij} \quad |\tau| \geq \tau_y, \quad (1)$$

$$d_{ij} = 0 \quad |\tau| < \tau_y, \quad (2)$$

where  $d_{ij}$  is the rate-of-deformation tensor [ $1/2((\partial v_i/\partial x_j) + (\partial v_j/\partial x_i))$ ],  $v_i$  is the velocity field,  $x_i$  is the coordinate and  $\dot{\gamma}$  is the rate of shear ( $(2d_{ij}d_{ij})^{1/2}$ ).  $\eta_0$  is the constant viscosity and  $\tau_{ij}$  is the deviatoric part of the inelastic non-Newtonian stress tensor. We have decomposed the total stress  $\sigma_{ij}$  into an isotropic pressure term and an extra-stress or deviatoric contribution, thus

$$\sigma_{ij} = -p\delta_{ij} + \tau_{ij}. \quad (3)$$

Here  $\delta_{ij}$  is the unit tensor and  $p$  is the isotropic pressure.

## 2. Numerical modelling

The present report considers the computer modelling of three-dimensional flows in inelastic materials with yield using a biviscosity differential formulation. For materials with yield and viscoelastic behaviour we refer readers to White and Tanaka [3] and White [4], who have developed plastic-viscoelastic constitutive equations, principally for particle-reinforced systems incorporating a yield value and using an integral formulation.

Defining a numerical criterion that identifies the onset of yielding requires formulation of a constitutive equation. One can approach the problem of writing down constitutive models for such materials from the classical theory of plasticity [5] and set up a yield criterion. The Tresca yield criterion assumes that flow begins when the maximum shear stress exceeds the shear yield stress. The most common three-dimensional constitutive relation uses the von Mises criterion for yielding which predicts that the material flows and deforms significantly only when the second invariant of the stress tensor exceeds the yield stress; otherwise the material behaves like a strained solid. Explicitly, the von Mises criterion used here is defined by

$$2\Pi \equiv \tau_{ij}\tau_{ij} > 2\tau_y^2 \quad (4)$$

Both schemes express yield in terms of a stress invariant which is computationally awkward in velocity–pressure finite-element schemes where typically one solves for velocity components and then for shear rates. Numerical noise masks the exact location of rigid cores wherein the stresses remain indeterminate and so the following alternative approach has been adopted whereby the rate of deformation invariant is used as the criterion for the onset of yielding. Another approach to computing with Bingham models is that of Beris et al. [6] who used a mixed method and retained stresses as well as velocities as unknowns; we shall not follow this excellent work as it greatly increases the number of unknowns.

Here we assume that at very low shear rates the material behaves as a highly viscous liquid, viscosity  $\eta_r$ , and that above a critical shear rate ( $\dot{\gamma}_c$ ) a transition in behaviour occurs, namely yielding. After yielding, the fluid takes on the apparent viscosity,  $\eta_0 + (\tau_y/\dot{\gamma})$ . This biviscosity model is a convenient method of modelling materials with yield stress and was adopted by Milthorpe and Tanner [7], O'Donovan and Tanner [8] and Beverly and Tanner [9]. The one-dimensional response is shown in Fig. 1. The initial viscous region can be made as steep as one wishes. Now the criterion for yielding is that a critical shear rate  $\dot{\gamma}_c$  is exceeded:

$$2d_{ij}d_{ij} > \dot{\gamma}_c^2. \quad (5)$$

We shall define  $|\dot{\gamma}|^2$  as the quantity on the left-hand side of (5). No longer is it necessary to distinguish computationally between a state of absolute rigidity ( $\dot{\gamma} = 0$ ) and a state of shear ( $\dot{\gamma} > 0$ ) as is necessary for the implementation of a true Bingham model. The yield point in terms of the rate of deformation is set by the fluid yield stress,  $\tau_y$ , and the choice of  $\eta_r$ , the high “reference” viscosity. By adopting this technique the viscosity curve remains continuous and smooth as opposed to the discontinuous curve representing the Bingham model.

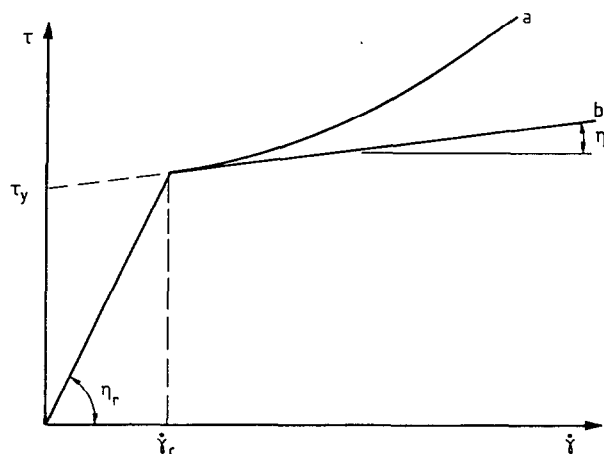


Fig. 1. One-dimensional yielding response for (a) a modified Herschel-Bulkley fluid; (b) a Bingham fluid, where  $\tau_y$  is the yield stress,  $\eta_0$  the viscosity and  $\eta_r$  the “unyielded” viscosity.  $\dot{\gamma}_c$  is the critical shear rate in the biviscosity model.

The one-dimensional law for the modified Bingham material requires that the viscosity be determined according to

$$\eta = \eta_r \quad |\dot{\gamma}| \leq \dot{\gamma}_c, \quad (6)$$

$$\eta = \eta_0 + \frac{\tau_y}{\dot{\gamma}} \quad |\dot{\gamma}| > \dot{\gamma}_c. \quad (7)$$

After some experimentation, we have set  $\eta_r$  to three orders of magnitude greater than  $\eta_0$ ; there is some latitude in this figure (see below). It also is important to note that if stresses (or  $\dot{\gamma}$ ) are everywhere very low compared to  $\tau_y$  (or  $\dot{\gamma}_c$ ) then misleading velocity fields can result from the biviscosity model. These situations should be avoided. The three-dimensional analogues of (6) and (7) require that

$$\tau_{ij} = \sigma_{ij} + p\delta_{ij} \equiv 2\eta_r d_{ij} \quad |\dot{\gamma}| \leq \dot{\gamma}_c, \quad (8)$$

$$\tau_{ij} = 2\left(\eta_0 + \frac{\tau_y}{|\dot{\gamma}|}\right) d_{ij} \quad |\dot{\gamma}| > \dot{\gamma}_c. \quad (9)$$

In order to obtain a plastic-viscoelastic material description the stress  $2\tau_y d_{ij}/\dot{\gamma}$  is added to the chosen viscous constitutive model, if and only if the critical shear rate has been exceeded, as reported in Ref. 9.

Note that in the limit of  $d_{ij} = 0$  the deviatoric stress becomes zero and so eqns. (8) and (9) are not consistent with the Bingham model, which merely predicts  $\tau \leq \tau_y$ . It must be emphasised that eqns. (8) and (9) do not reduce to the Bingham model in the limit  $\dot{\gamma} = 0$ ; for  $\dot{\gamma} > \dot{\gamma}_c$  they are believed to be an excellent approximation, as mentioned above.

Recently Ellwood et al. [10] reported encouraging results using the following constitutive equation proposed by Papanastasiou [11]

$$\tau = 2 \left\{ \mu + \frac{\tau_y}{\sqrt{2\Pi_D}} \left[ 1 - \exp(-m\sqrt{\Pi_D}) \right] \right\} D, \quad (10)$$

where  $\Pi_D$  is the second invariant of the rate of strain tensor  $D$  and  $m$  is a stress growth exponent; the von Mises criterion is approximated for relatively large exponents of  $m$ . Equation (10) approximates well the ideal Bingham liquid as will be demonstrated in the discussion of the results. Clearly

$$\eta = \mu \quad \dot{\gamma} \gg 1, \quad (11)$$

$$\eta = \mu + m\tau_y \quad \dot{\gamma} \rightarrow 0. \quad (12)$$

From the computational point of view eqn. (10) is simple to implement, holds uniformly in yielded-and unyielded regions and derives good approximations in the limit of low shear rates. A smooth continuous transition from a state of infinitely high viscosity to one of yielding is assured with careful selection of the exponential growth parameter  $m$ . However, unlike the biviscosity model, this smoothness does obscure the clear line between yielded and unyielded regions. Overall, it is questionable whether this model is superior to a non-Newtonian model which predicts similar flow characteristics.

Unless otherwise stated, all comments and data presented in this paper refer to, and are derived using, the biviscosity model described earlier.

### 3. Selection of a finite element

In order to formulate a finite-element scheme we introduce within each element velocity and pressure approximations defined by

$$v_j^e = \sum_i N^i(\xi, \eta, \zeta) v_j^i, \quad (13)$$

$$p^e = \sum_i N_p^i(\xi, \eta, \zeta) p^i, \quad (14)$$

where  $v_j^i$  and  $p^i$  are the nodal velocity and pressure values respectively. The interpolation (basis) functions  $N^i$  and  $N_p^i$  are defined within each Lagrangian element with respect to the local  $(\xi, \eta, \zeta)$  coordinate system. For continuity enforcement, it has been established that the pressure basis function,  $N_p^i$ , should always be at least one order lower than that used for velocities,  $N^i$  (see Hood and Taylor [12] for details). This condition is valuable in eliminating some unsuitable element configurations but it is not

sufficient to ensure stability and accuracy of the numerical solution. The key requirement is satisfaction of the Brezzi and Babuska (B.B.) condition.

From Brezzi (see Ref. 12), stability of finite-element approximations requires that the following inf-sup condition be satisfied for a constant  $\alpha$  independent of  $h$

$$\inf \sup \frac{b(v_h, q_h)}{v_h^V q_h^P} \geq \alpha, \quad (15)$$

where  $v_h$  and  $q_h$  denote the finite dimensional spaces of trial functions for the finite-element solutions of  $u^h$  and  $p^h$  respectively. The bilinear form  $b(.,.)$  defines an operator  $B_h$  from  $x_h$  onto  $q_h$ . Stability requires that the space  $v_h$  be sufficiently large with respect to the space  $q_h$  whilst being small enough to maintain an optimum convergence rate for both velocity and pressure. Once an element has been chosen, the construction of the program used in the present investigation follows classical lines [13,14].

### 3.1. Three-dimensional incompressible elements

In the Galerkin formulation of generalised Newtonian incompressible flow, the pressure trial function must be at least an order lower than the velocity approximation, on the basis of stability and accuracy considerations. This rule eliminates some unsuitable element configurations but is not sufficient to ensure that numerical pressure fields will be free of non-physical oscillations. The essential requirement is satisfaction of the B.B. condition which requires that the finite dimensional spaces of velocity trial functions are sufficiently large compared to those corresponding to pressure trial functions whilst ensuring optimum convergence rates for both velocity and pressure.

A detailed study of the stability, accuracy and computational overheads of well-known and widely used three-dimensional compressible elements has been reported by Beverly and Tanner [15]. It was found that often the three-dimensional analogues to successful two-dimensional elements did not satisfy the B.B. condition. Indeed, the most basic three-dimensional elements lacked the essential mass control feature in order to satisfy the B.B. condition whereas the triquadratic family of elements requires large amounts of computational space and execution time.

The fifteen-noded "enriched" trilinear family of elements proposed by Fortin [16] and Fortin and Fortin [17] provided the necessary mass control features to eliminate parasitic pressure modes and preserve elementwise continuity, thereby satisfying the B.B. condition. The interpolation for velocity is an "enriched" linear (or incomplete quadratic); pressure is

TABLE 1

Summary of viscous three-dimensional elements

Element	$v$ -Nodes	$p$ -Nodes	Convergence	Ratio	B.B.
Trilinear	8	1	$O(h)$	1/3	No
Trilinear	9	1	$O(h)$	1/6	No
Inc. Quad. <sup>a</sup>	20	1	$O(h)$	1/12	No
Inc. Quad.	20	8	$O(h^2)$	1/12	Yes
Inc. Quad.	20	9	$O(h^2)$	1/6	Yes
Inc. Quad.	21	8	$O(h^2)$	1/15	Yes
Inc. Quad.	21	9	$O(h^2)$	2/15	Yes
Quadratic	27	8	$O(h^2)$	1/24	Yes
Quadratic	27	9	$O(h^2)$	1/12	Yes
Enrh. Lin. <sup>b</sup>	15	1	$O(h)$	1/15	Yes
Enrh. Lin.	15	4	$O(h)$	1/5	Yes
Enrh. Lin.	15	4	$O(h)$	1/5	Yes

Ratio refers to the constraint ratio which is the ratio of continuity equations per element to momentum equations per element (after boundary conditions have been imposed) as the number of elements per side approaches infinity. A small ratio implies poor enforcement of the divergence-free constraint.

<sup>a</sup> Incomplete quadratic.

<sup>b</sup> Enriched linear.

piecewise constant. To date this element has proved to perform within acceptable limits of accuracy whilst maintaining a low computational time overhead. The discontinuous pressures permit modelling of composite material problems which otherwise are not possible with continuous pressure elements. Since the yield surface is similar to a composite material interface, the discontinuous pressures are useful for Bingham flows.

A summary of element types considered is given in Table 1.

#### 4. Test case one: Poiseuille flow

The accuracy of the biviscosity algorithm (9) versus the constitutive equation proposed recently by Ellwood et al. (10) was assessed by computing the simple plane channel flow of a Bingham material [2] using several elements. For each solution we computed the error measure  $\sqrt{\sum_n (V - V_{\text{exact}})^2} / \sqrt{\sum_n V_{\text{exact}}^2}$  where  $n$  is the number of nodes and the exact solution is known [18]. In this test case the number of iterations was fixed thereby avoiding the often unstable Newton–Raphson approach; the rate of convergence was thereby easily accessed.

We looked at the case of varying  $\eta_r$  (Table 2). Small changes in accuracy were noted with the planar problem using a fixed grid as  $\eta_r/\eta_0$  was varied

TABLE 2  
Sensitivity of algorithm to various choices of reference viscosity when compared with the exact (Poiseuille) solution for Bingham flow

Grid	Type	$\eta_r$	Velocity RMS
$6 \times 10$	Planar	$1000\eta_0$	$0.1750\text{E}-3$
$21 \times 21$	Planar	$10\eta_0$	$0.2239\text{E}-4$
		$100\eta_0$	$0.2267\text{E}-5$
		$1000\eta_0$	$0.1962\text{E}-5$
		$10\,000\eta_0$	$0.1762\text{E}-5$
$6 \times 10$	Axisymmetrical	$1000\eta_0$	$0.1729\text{E}-2$
$21 \times 21$	Axisymmetrical	$10\eta_0$	$0.1701\text{E}-2$
		$100\eta_0$	$0.1868\text{E}-4$
		$1000\eta_0$	$0.8654\text{E}-5$
		$10\,000\eta_0$	$0.1002\text{E}-4$

from 10 to  $10^4$ . With an axisymmetric (tube flow) problem, the highest accuracy was obtained when  $\eta_r/\eta_0$  was about 1000. This value has therefore been used in the work below.

To show the effect of mesh variations and element changes some results are shown in Tables 3–5, which have been compiled for various meshes. For equal accuracy of solution, the computational times in Tables 3–5 give a measure of element efficiency; Fig. 2 graphically represents Table 3 data. The errors shown in Tables 3–5 and Fig. 2 were computed for two meshes:

TABLE 3  
Planar Bingham plug flow <sup>a</sup>

No.	Element <sup>b</sup>	No. of elements	No. of nodes	Error measure	CPU
10	15(con.)	60	470	$0.3804\text{E}-2$	0:18:10
11	15(dis.)		470	$0.2832\text{E}-2$	0:24:15
12	19		710	$0.2790\text{E}-2$	0:21:20
7	21		563	$0.2714\text{E}-2$	0:51:06
9	27	120	819	$0.2619\text{E}-2$	1:16:21
10	15(con.)		920	$0.2636\text{E}-2$	0:39:23
11	15(dis.)		920	$0.1831\text{E}-2$	0:49:53
12	19		1400	$0.1742\text{E}-2$	0:45:51
7	21		1093	$0.2076\text{E}-2$	2:03:04
9	27		1599	$0.1961\text{E}-2$	3:04:58

Computations involved 25 iterations and were performed on an Ardent Risc6000 series machine; CPU time in hours:minutes:seconds. The error measure is  $\sqrt{\sum_n (V - V_{\text{exact}})^2} / \sqrt{\sum_n V_{\text{exact}}^2}$  where  $n$  is the number of nodes.

<sup>a</sup>  $\tau = 0.15 + 0.33 \dot{\gamma}$ ;  $\eta_+ = 1000\eta_0$ .  
<sup>b</sup> con. = continuous; dis. = discontinuous.



TABLE 4

Planar Bingham plug flow <sup>a</sup>

No.	Element <sup>b</sup>	No. of elements	No. of nodes	Error measure	CPU
10	15(con.)	60	470	0.9274E-2	0:18:10
11	15(dis.)		470	0.5263E-2	0:24:15
12	19		710	0.5059E-2	0:21:20
7	21		563	0.4531E-2	0:51:06
9	27		819	0.3619E-2	1:16:21
10	15(con.)	120	920	0.6427E-2	0:39:23
11	15(dis.)		920	0.3403E-2	0:49:53
12	19		1400	0.3159E-2	0:45:51
7	21		1093	0.2741E-2	2:03:04
9	27		1599	0.2561E-2	3:04:58

Computations involved 25 iterations and were performed on an Ardent Risc6000 series machine; CPU time in hours:minutes:seconds. The error measure is  $\sqrt{\sum_n (V - V_{\text{exact}})^2} / \sqrt{\sum_n V_{\text{exact}}^2}$  where  $n$  is the number of nodes.

<sup>a</sup>  $\tau = 0.15 + 0.33 \dot{\gamma}$ ; Papanastasiou  $m = 20$ .

<sup>b</sup> con. = continuous; dis. = discontinuous.

60 and 120 elements total, with 10 and 20 elements across the channel width respectively. Error measure was reduced with grid refinement. For a given accuracy the 15-node elements are seen to be the most economical in time. For example, in line 5 of Table 3, the 60-element computation with

TABLE 5

Planar Bingham plug flow <sup>a</sup>

No.	Element <sup>b</sup>	No. of elements	No. of nodes	Error measure	CPU
10	15(con.)	60	470	0.2739E-2	0:18:10
11	15(dis.)		470	0.1232E-2	0:24:15
12	19		710	0.1352E-2	0:21:20
7	21		563	0.8853E-3	0:51:06
9	27		819	0.7269E-3	1:16:21
10	15(con.)	120	920	0.1898E-2	0:39:23
11	15(dis.)		920	0.7965E-3	0:49:53
12	19		1400	0.8440E-3	0:45:51
7	21		1093	0.7265E-3	2:03:04
9	27		1599	0.6684E-3	3:04:58

Computations involved 25 iterations and were performed on an Ardent Risc6000 series machine; CPU time in hours:minutes:seconds. The error measure is  $\sqrt{\sum_n (V - V_{\text{exact}})^2} / \sqrt{\sum_n V_{\text{exact}}^2}$  where  $n$  is the number of nodes.

<sup>a</sup>  $\tau = 0.15 + 0.33 \dot{\gamma}$ ; Papanastasiou  $m = 1000$ .

<sup>b</sup> con. = continuous; dis. = discontinuous.

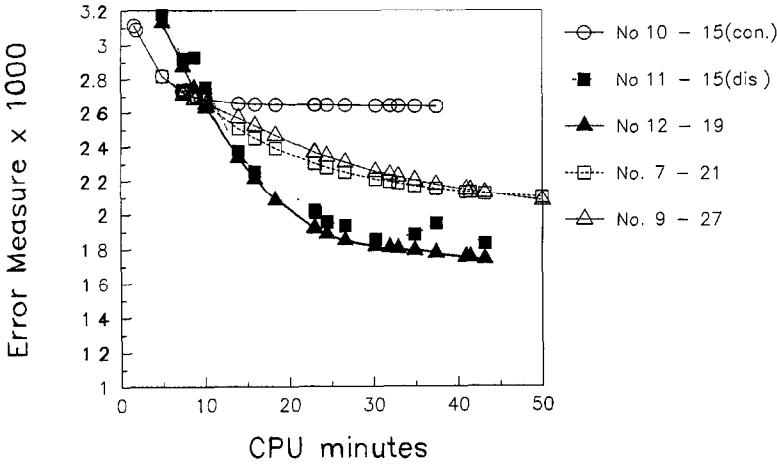


Fig. 2. Comparative error analysis of several three-dimensional elements derived from a fully-developed planar Bingham plug flow problem. Error measure is defined by  $\sqrt{\sum_n (V - V_{\text{exact}})^2} / \sqrt{\sum_n V_{\text{exact}}^2}$  where  $n$  is the number of nodes and the exact solution is known [18]. Computations were performed on an Ardent Risc6000 series machine; CPU time in minutes.

the 27-node brick took 1 h 16 min 21 s and produced an accuracy measure of  $0.2619 \times 10^{-2}$ , while the 15-node (discontinuous) brick with 120 elements produced an accuracy of  $0.1831 \times 10^{-2}$  in only 49 min 53 s. With a given grid, namely the 120 element mesh, Fig. 2 compares CPU times and accuracy. For a specific CPU time we see that the 15-node element gives more accuracy than the others. This good performance was evident in all cases examined below. In more complex problems the superior performance of the Fortin 15-node elements was even more marked; in some cases computations with the 27-node element were infeasible due to long run times and excessive storage. The economy of the Fortin 15-node elements for a given accuracy is striking.

Tables 4 and 5 also show the effect of using the Papanastasiou “yield” function (11). The errors are somewhat greater for  $m = 20$  than with the biviscosity scheme; for  $m = 1000$  the error measure is reduced. Computational times are similar in all cases using the same element configuration.

### 5. Test case two: axial flow of a Bingham fluid in an annulus

Fredrickson and Bird [19] derived an analytical solution for this problem, an outline of which is given below. The problem statement is to determine the velocity distribution, and bounds of the plug-flow region, of a Bingham fluid flowing through the annular gap between two coaxial cylinders of radii  $\kappa R$  and  $R$ ;  $\kappa R$  is the radius of the inner cylinder ( $0 < \kappa < 1$ ).

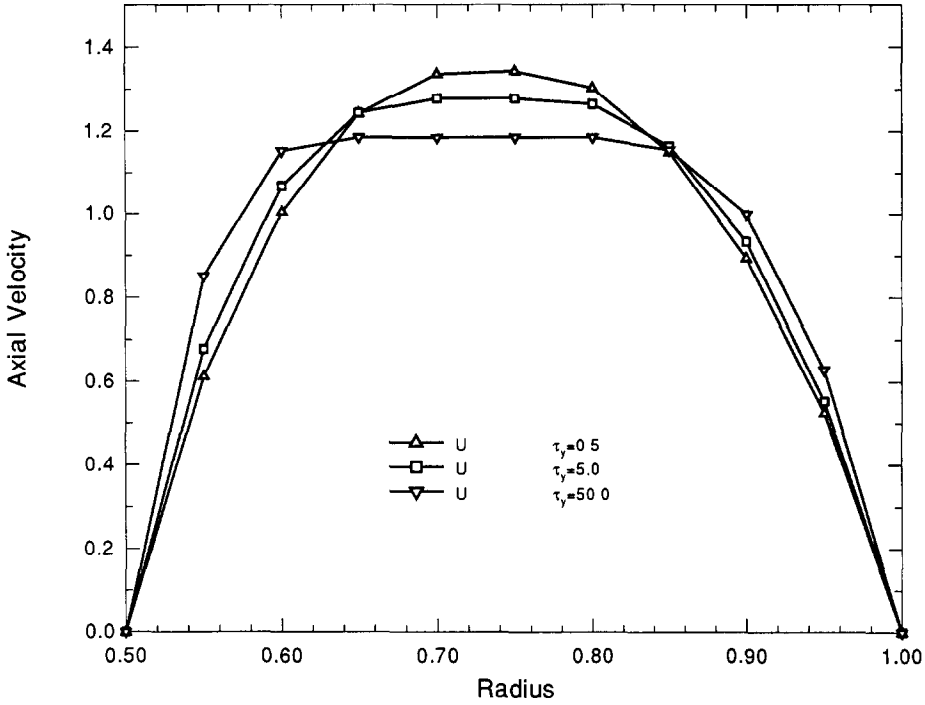


Fig. 3. Axial velocity distribution for a series of Bingham fluids flowing through an annulus. With a constant flow rate and increasing yield stress the bounds of the plug-flow region increase and the plug zone becomes more pronounced. In all cases  $\eta_0 = 1$ ,  $R = 1$  and  $\kappa = 0.5$ .

The solution is considerably simplified by introducing the dimensionless variables

$$T = \frac{2\tau_{rz}L}{(P_0 - P_L)R}, \quad (16)$$

$$T_0 = \frac{2\tau_0L}{(P_0 - P_L)R}, \quad (17)$$

$$V = \left[ \frac{2\eta_0L}{(P_0 - P_L)R^2} \right] v_z, \quad (18)$$

$$\zeta = r/R, \quad (19)$$

where  $T$  represents a dimensionless shear stress,  $T_0$  is a dimensionless yield stress,  $V$  a dimensionless velocity and  $\zeta$  is a dimensionless radial

distance as measured from the annulus axis. The bounds of the plug-flow region  $\beta_+$  and  $\beta_-$  are given by

$$\pm T_0 = \beta_{\pm} - \left( \frac{\beta_{\pm}^2}{\beta_{\pm}} \right), \quad (20)$$

where  $\beta$  is a constant of integration.

It can be shown that the dimensionless velocity for the region between the core and the inner cylinder ( $\kappa \leq \zeta \leq \beta_-$ ) is given by

$$V_- = T_0(\kappa - \zeta) - \frac{1}{2}(\zeta^2 - \kappa^2) + \beta^2 \ln\left(\frac{\zeta}{\kappa}\right). \quad (21)$$

Similarly for the region between the solid core and the outer wall ( $\beta_+ \leq \zeta \leq 1$ )

$$V_+ = T_0(\zeta - 1) + \frac{1}{2}(1 - \zeta^2) + \beta^2 \ln(\zeta). \quad (22)$$

In the solid core ( $\beta_- \leq \zeta \leq \beta_+$ ) we must satisfy

$$V_0 = V_-(\beta_-) = V_+(\beta_+). \quad (23)$$

In order to determine the outer radius of the plug we must solve the determining equation

$$2\beta_+(\beta_+ - T_0) \ln\left(\frac{\beta_+ - T_0}{\beta_+ \kappa}\right) - 1 + (T_0 + \kappa)^2 + 2T_0(1 - \beta_+) = 0, \quad (24)$$

from which the inner radius and constant of integration then follow from eqn. (20) to be

$$\beta_- = \beta_+ - T_0 \quad (25)$$

and

$$\beta^2 = \beta_- \beta_+. \quad (26)$$

Figure 3 shows the velocity distribution for a series of Bingham fluids with increasing yield stress, showing how the solid core varies when the yield stress is varied.

## 6. Flow of a Bingham fluid in an eccentric annulus

Of practical importance to the oil and gas industry is the characterisation of drilling mud as it moves axially along a borehole between the casing and the wellbore walls. The drilling mud, as with the cement slurries used to form an impermeable barrier between the casing and the rock, are generally regarded as non-Newtonian suspensions exhibiting apparent yield

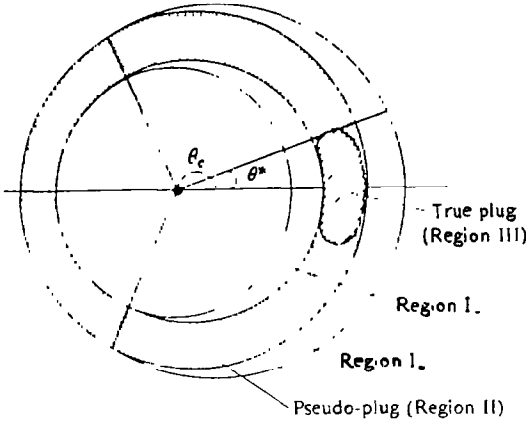


Fig. 4. Flow regions in an annulus as characterised by Walton and Bittleston [21].

stress. To a first approximation, these fluids may be characterised by the Bingham model.

Pearson [20] considered the idealisation of an eccentric annular gap between casing and formation, the inner metal cylinder neither reciprocating axially or rotating about its own axis. A modified Bingham constitutive equation was used to identify analytically axial velocity stationary, plug and slowly distorting regions.

A more rigorous analytic solution was presented by Walton and Bittleston [21] based on the narrow-gap approximation. This solution is equivalent, at least to a first approximation, to neglecting the effects of curvature and treating the annulus as if it were a slot of variable width. The leading-order solution divides the annulus into a number of regions in each of which a different form of solution must be found. Three regions were characterised (as in Fig. 4). Region I lies outside a pseudo-plug zone and represents a slowly distorting transition or shearing region, Region II is an extension of the central pseudo-plug and Region III represents the true plug zone. Within Region I the stress is greater than the yield stress and the axial velocity remains constant across it but not along it. It was theorised that true plugs existed at the widest (and under certain conditions at the narrowest) part of the annulus, their azimuthal extent depending on the eccentricity,  $e$ , of the annulus. Their results supported those of Pearson [20].

For convenience, and consistency of nomenclature with that adopted in Ref. 21, we define a normalised parameter, called the Bingham number  $Bn$ , by

$$Bn = \frac{\tau_y d}{\mu_0 w_0}, \quad (27)$$

where  $w_0$  is a reference velocity,  $d$  is some characteristic dimension taken to be the difference in the radii of the two bounding cylinders,  $\mu_0$  is a reference viscosity and  $\tau_y$  is the yield stress. The dimensionless gap width,  $\delta$ , is normalised relative to the inner cylinder radius,  $r_i$ , via

$$\delta = d/r_i. \quad (28)$$

In our approach using the finite-element method, a constant flow rate criterion is used, contrary to the constant pressure gradient scheme used by Walton and Bittleston [21].

As a natural extension to the above idealisation of an eccentric annular gap between casing and formation, results will also be presented for the case where the inner cylinder rotates about its own axis at a constant angular velocity of  $v_\theta = 1.0$ . Such a situation presents a more realistic representation of the drilling process and necessitates a full discretisation of the well.

### 6.1. Numerical results

In order to compare results presented by other researchers [20,21] and to gain an appreciation of different flow patterns, numerical results were derived using four different regimes: Newtonian, Carreau, Power-law and Bingham. Figure 5 shows constant axial velocity contours in an annulus with radius ratio 0.5, eccentricity of 0.5 and an outer cylinder radius of 0.5. Cross-sectional profiles are compiled from results two diameters downstream, the total wellbore length being four diameters. There are ten equally spaced contour values, increasing in magnitude from contour level one to contour level ten. The overall range of the contour values is scaled between zero and the peak Newtonian velocity. Figure 5(a) shows the response of a Newtonian fluid. Symmetry exists about the mean radius and the flow is fastest through the wide side of the annulus. The flow rate decays as one proceeds toward the narrow side of the annulus. Figure 5(b) shows the flow pattern of a Carreau fluid with index 0.5 and infinite viscosity  $\eta_\infty = 0$ . Clearly, the shear rates near the wall have increased compared to the Newtonian results. The extent of the fast-moving region on the wide side of the annulus has increased and extends further around the annulus towards the narrow side. The narrow side supports a reduced flow rate relative to the Newtonian regime. Figure 5(c) shows the flow pattern of a Power-law fluid with index 0.5 which behaves similarly to the Carreau material. Figure 5(d) shows the flow pattern of a Bingham material with a normalised  $Bn$  parameter of 25. The deviations from the Newtonian solution displayed by the Power-law regime have intensified

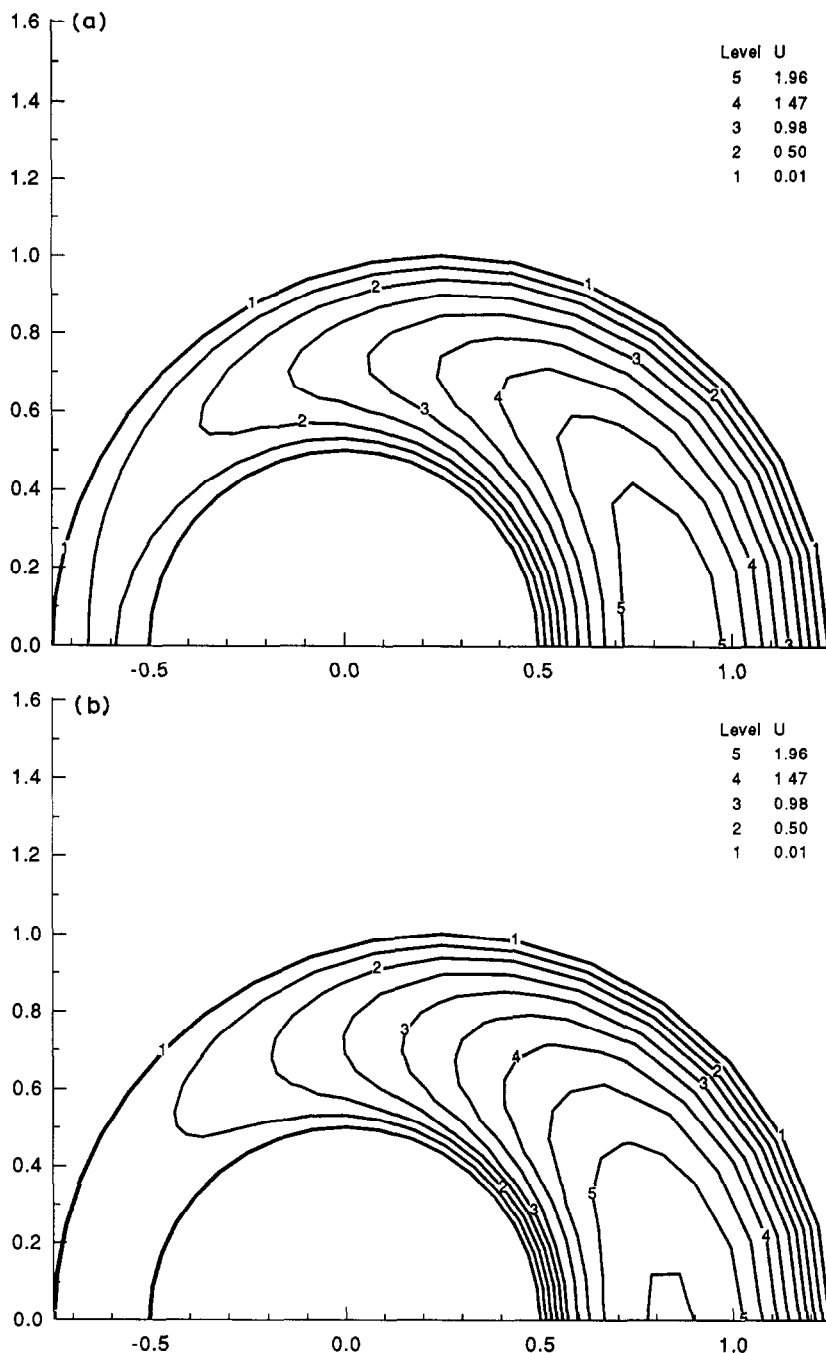


Fig. 5. Axial velocity contours of (a) a Newtonian fluid, (b) a Carreau fluid; (c) a Power-law fluid; (d) a Bingham fluid in an annulus with radius ratio of 0.5 and offset 0.5. Cross-sectional profiles are compiled from numerical results two diameters downstream, the total wellbore length being four diameters.

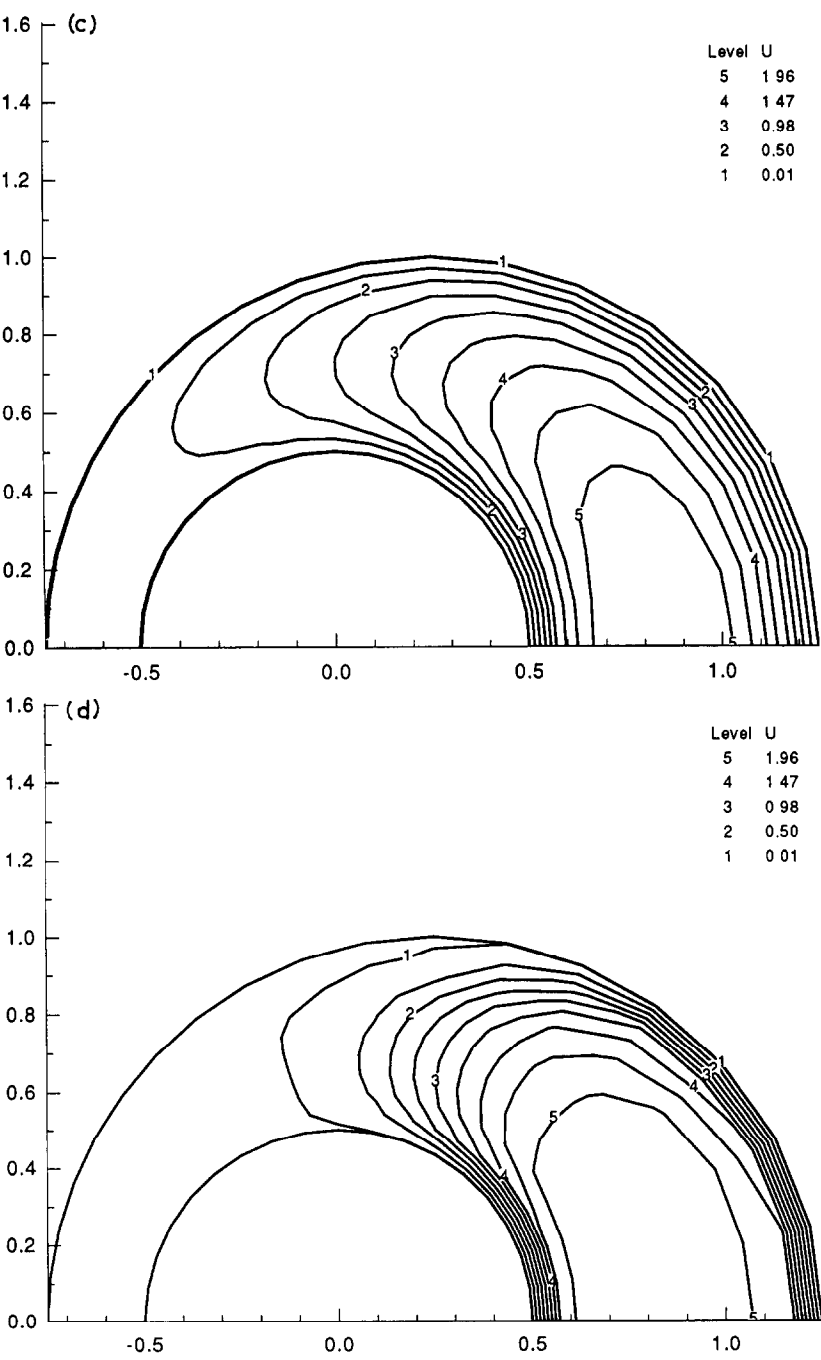


Fig. 5 (continued).



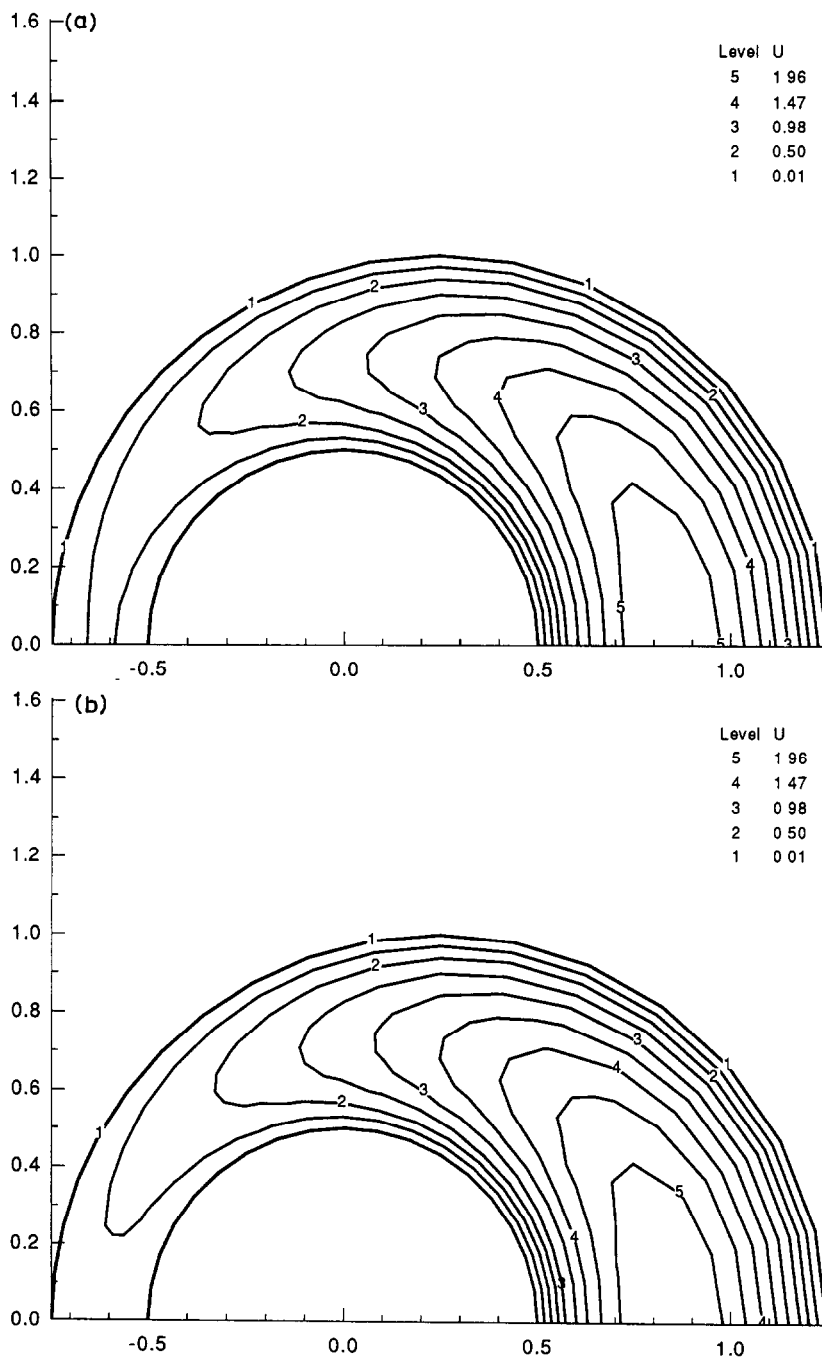


Fig. 6. Axial velocity contours of (a) a Newtonian fluid; (b, c, d, e) a series of Bingham materials in an annulus with radius ratio of 0.5 and offset 0.5. Cross-sectional profiles are compiled from numerical results two diameters downstream, the total wellbore length being four diameters. In all cases the inner cylinder is stationary and the mass flux is constant. The yield stress increases as follows:  $\tau_y = 0.5$  (b);  $\tau_y = 5.0$  (c);  $\tau_y = 50.0$  (d);  $\tau_y = 500.0$  (e).

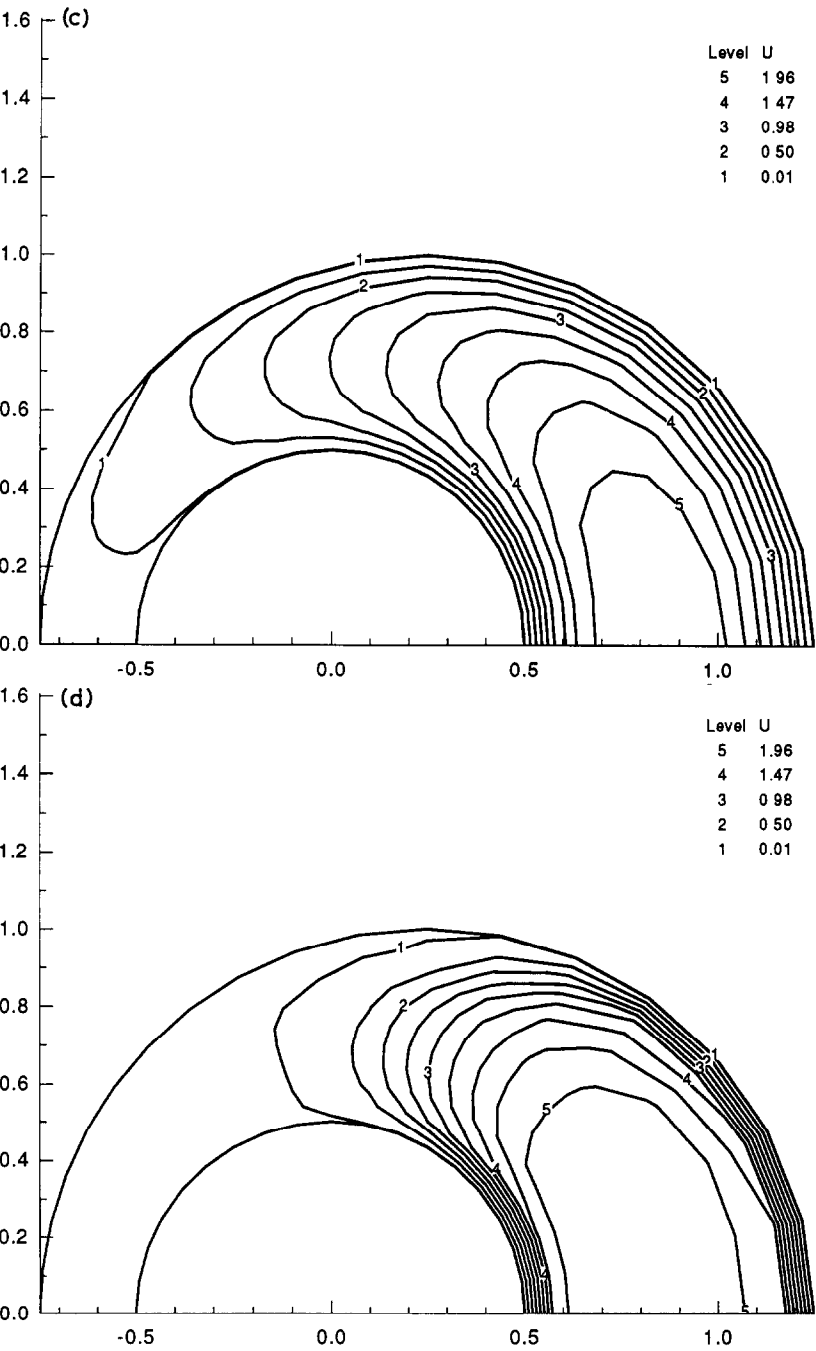


Fig. 6 (continued).

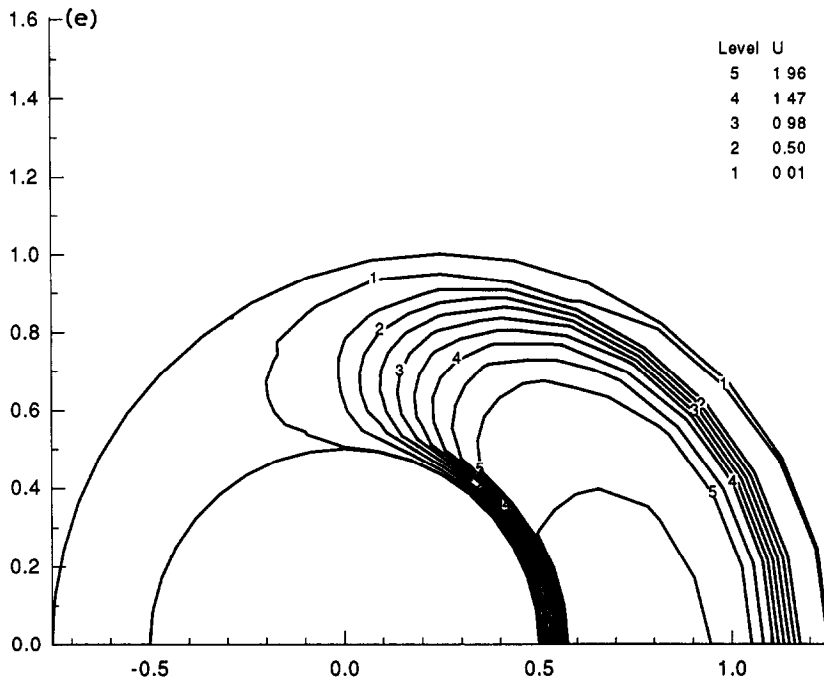


Fig. 6 (continued).

with a large plug region existing on the wide side of the annulus. Very high shear rates occur near the walls.

Figure 6 shows five flow patterns for a series of Bingham materials ranging in normalised  $Bn$  numbers from 0.25 to 250; the Newtonian case is also shown and acts as a standard against which comparisons can be drawn. In all cases the annulus configuration and contour values are as described in Fig. 5. With increasing  $Bn$  number the extent and magnitude of the plug region (Region III) increases on the wide side of the annulus so as to enforce the continuity equation and preserve mass flow rate. Concurrently, once a critical  $Bn$  value has been exceeded the extent of the stationary zone (Region II) increases on the narrow side of the annulus. This critical  $Bn$  value occurs when the pseudo-plug (Region II) fully occupies the narrow gap. Under these conditions the pseudo-plug region represents a stationary zone as the velocity of the fluid within this zone must satisfy the no-slip wall boundary conditions.

Figure 7 shows a series of centreline axial velocities as a function of angular position for the flow cases presented in Fig. 6. The angular position is measured in radians and is zero in the widest part of the annulus and  $\pi$  in the narrowest part. It is clear from the figure that the critical  $Bn$  number for this flow geometry and mass flow rate conditions occurs at

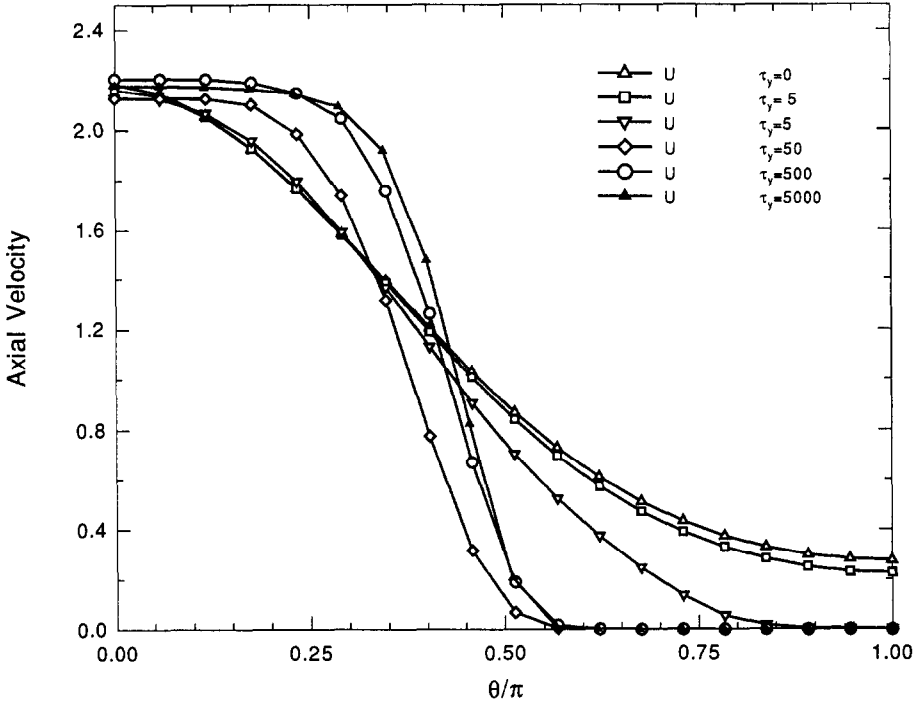


Fig. 7. Centreline (i.e. midway between the cylinders) axial velocities as a function of angular position for the flow cases presented in Fig. 6.

approximately 0.25; this is in agreement with the leading-order solution which defines this critical number to be  $\frac{1}{2}(1 - e)$  where  $e$  is the eccentricity ( $e = 0.5$  in this case). If  $Bn < \frac{1}{2}(1 - e)$  then the pseudo-plug is narrower than the narrowest part of the annulus and therefore extends all the way round; the axial velocity within this zone is non-zero and constant. If  $Bn > \frac{1}{2}(1 - e)$  then there is a critical angle,  $\theta_c$ , at which the thickness of the pseudo-plug is exactly equal to the gap thickness. Zones beyond this critical angle ( $\theta > \theta_c$ ) experience stationary axial flow. To a first approximation  $\theta_c$  was identified by Walton and Bittleston [21] to be

$$\theta_c = \cos^{-1} \left( \frac{2Bn - 1}{e} \right) \quad (29)$$

and holds well for the cases explored by them and observed in our results. Also, if  $Bn > \frac{1}{2}(1 - e)$  then true plug flow (Region III) forms in the region near  $\theta = 0$ , the widest part of the annulus. The extent of this plug region is defined

$$\theta^* = \left( \frac{6Bn^2\delta}{e} \right)^{1/3}. \quad (30)$$

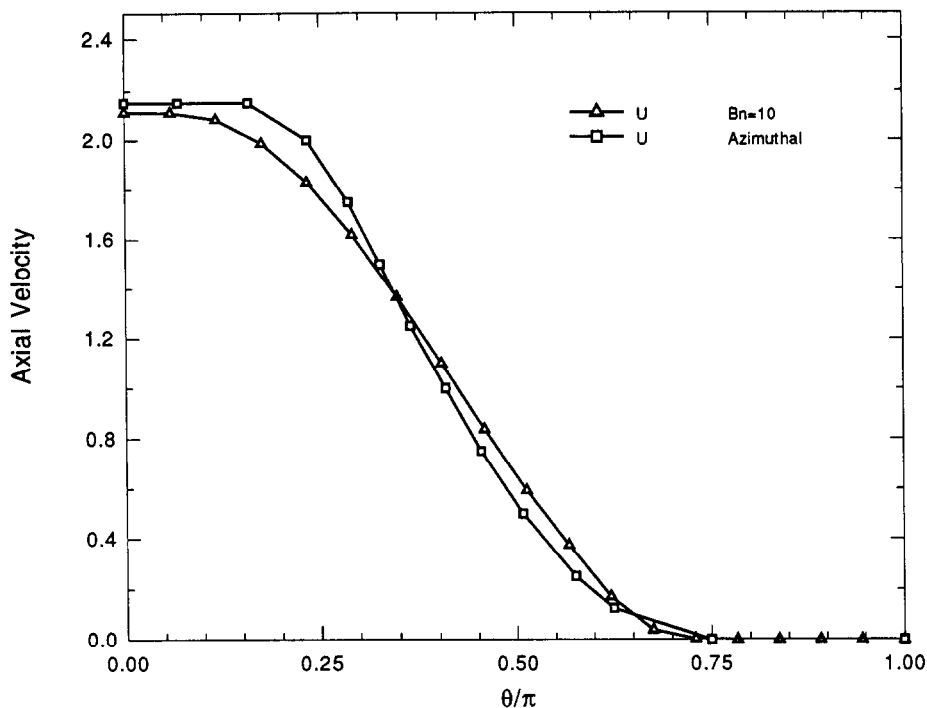


Fig. 8. Centreline axial velocity as a function of angular position for a Bingham fluid defined by  $Bn=10$ . Also shown is the typical azimuthal velocity distribution for this case, as reported by Walton and Bittleston [21].

Assuming constant geometry, with increasing  $Bn$  beyond the critical Bingham number the extent of the plug region should increase concurrently with an increase in the extent of the stationary zone; the transition zone between these limits necessarily occupies a smaller region. This prediction is observed in Fig. 7.

Figure 8 shows a plot of the centreline axial velocity as a function of angular position for the flow of a Bingham fluid in an annulus with parameter  $Bn = 10$ . The annulus configuration is as described in Fig. 5 and the numerical axial velocity solution is compiled from results two diameters downstream. The angular position is measured in radians and is zero in the widest part of the annulus and  $\pi$  in the narrowest part. Also shown in the figure is the typical azimuthal velocity distribution for this case, as reported by Walton and Bittleston [21]. This diagram demonstrates that good quantitative agreement exists between the numerical predictions and the narrow-gap approximations. It must be emphasised that Walton and Bittleston [21] encountered errors between their numerical scheme and the azimuthal solution of about 10% for  $\delta \approx 0.4$ ; larger errors were predicted with increasing  $\delta$ . Figure 8 depicts the case where  $\delta = 1.0$ .

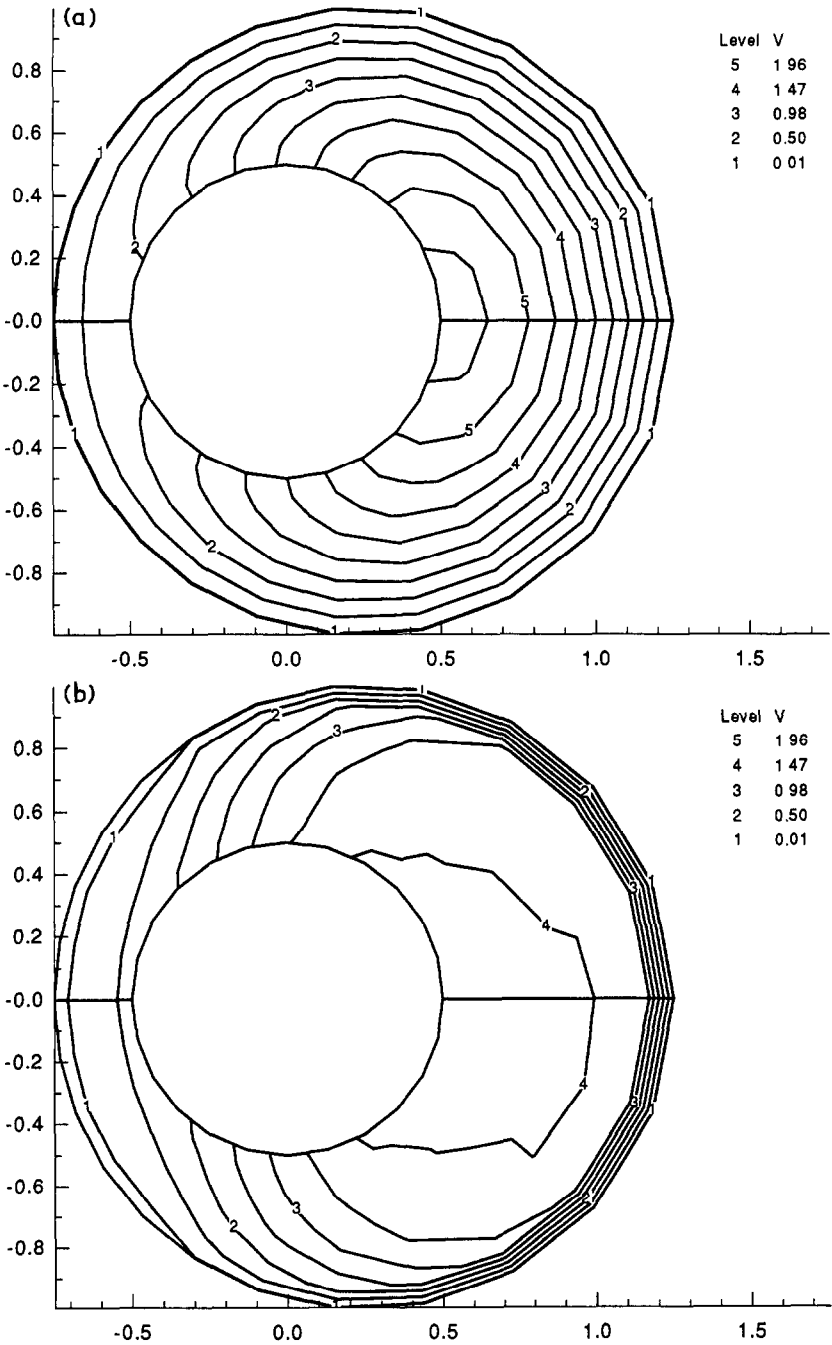


Fig. 9. Axial velocity contours of (a) a Newtonian fluid; (b) a Bingham fluid characterised by  $\tau_y = 50$  in an annulus with radius ratio of 0.5, offset 0.5 and the inner cylinder rotates about its own axis with a constant angular velocity of unity. Cross-sectional profiles are compiled from numerical results two diameters downstream, the total wellbore length being five diameters.

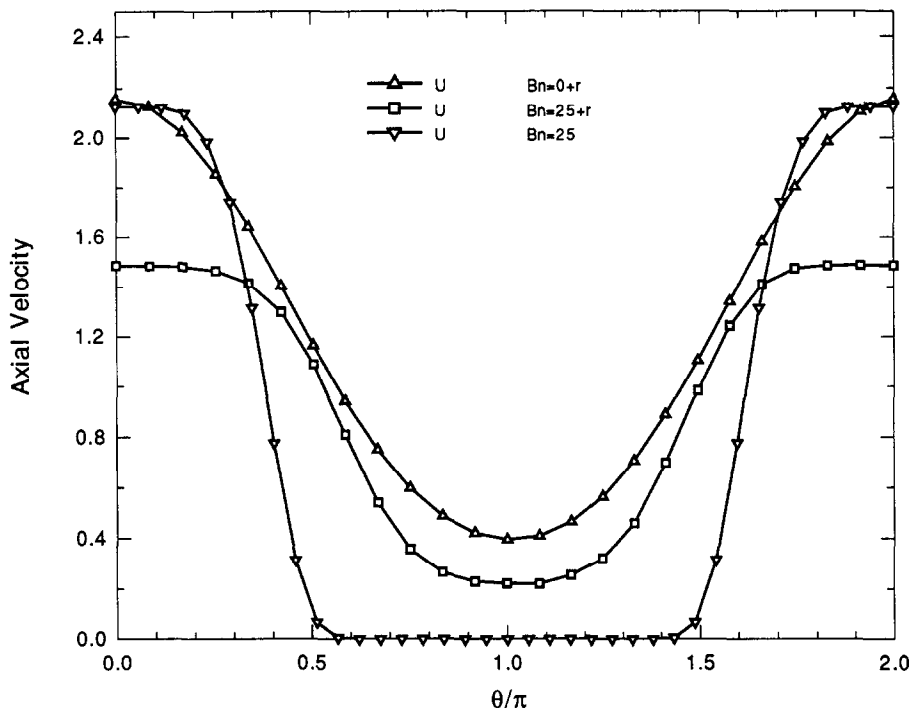


Fig. 10. Centreline axial velocities as a function of angular position for the flow cases presented in Fig. 9. The postscript '+r' refers to instances where the inner cylinder rotates about its own axis, otherwise the inner casing remains stationary.

Consider next the case where the inner cylinder rotates about its own axis with a constant angular velocity of unity. Figure 9 shows constant axial velocity contours in an annulus with radius ratio 0.5, eccentricity of 0.5 and an outer cylinder radius of 0.5. Cross-sectional profiles are compiled from results two diameters downstream, the total wellbore length being four diameters. There are ten equally spaced contour values, increasing in magnitude from contour level one to contour level ten. The overall range of the contour values is scaled between zero and the peak Newtonian velocity. Figure 9(a) shows the response of a Newtonian fluid. Symmetry exists about the mean radius and the flow is fastest through the wide side of the annulus. The flow rate decays as one proceeds toward the narrow side of the annulus. Figure 9(b) shows the flow pattern of a Bingham material with a normalised  $Bn$  parameter of 25.

Figure 10 shows a series of centreline axial velocity plots as a function of angular position for the flow of a Bingham fluid in an annulus. The annulus configuration is as described in Fig. 9 and the numerical axial velocity solution is compiled from results two diameters downstream. The angular

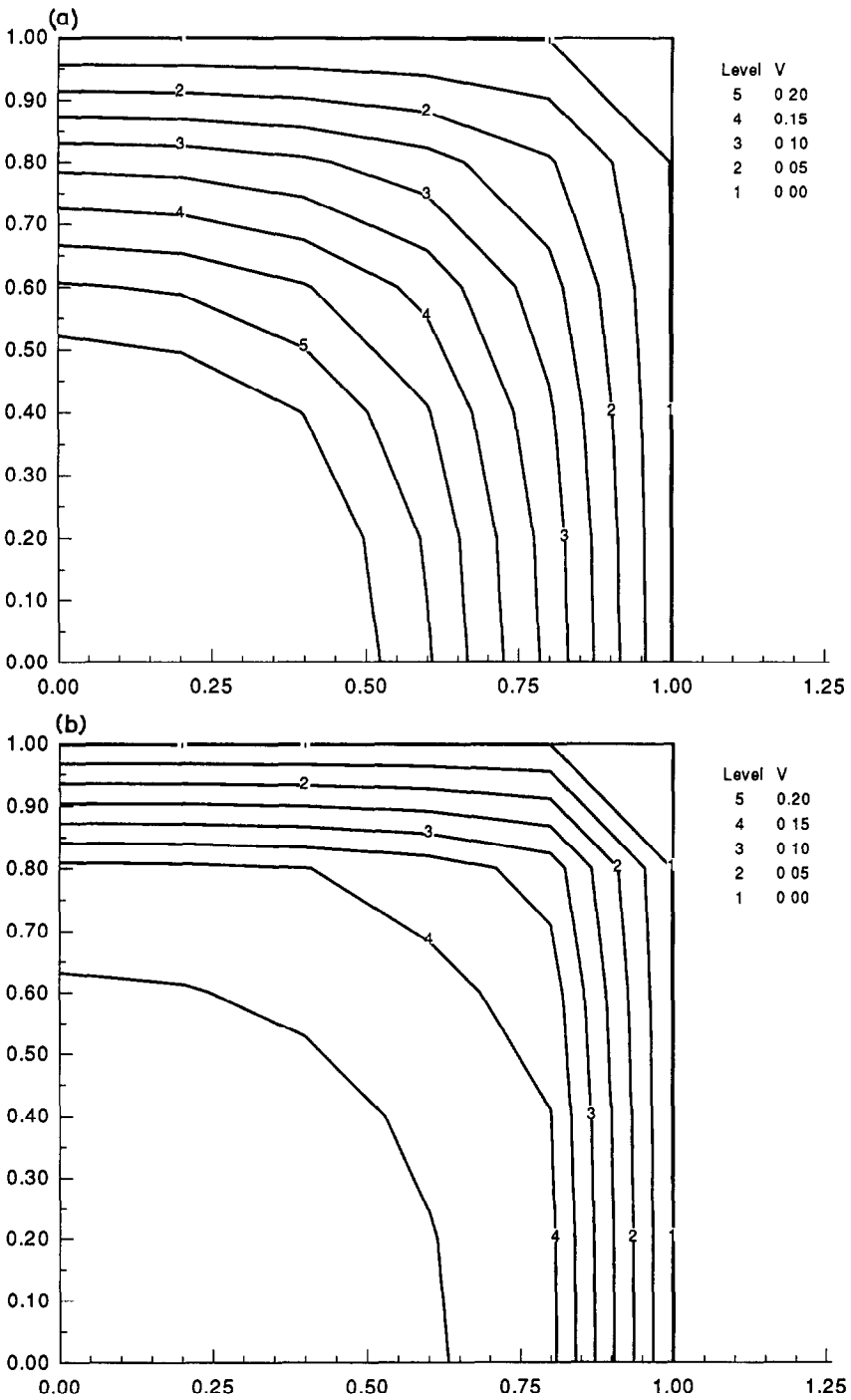


Fig. 11. Axial velocity contours of a Bingham material extruded through a square die where  $\tau_y = 0.5$ ,  $\bar{w} = 0.1395$  and  $\eta_0 = 1.0$ . Velocity contours are compiled across (a) the inlet  $x = 0$ ; (b) the exit plane  $x = 4$ ; (c) the free body  $x = 10$ .



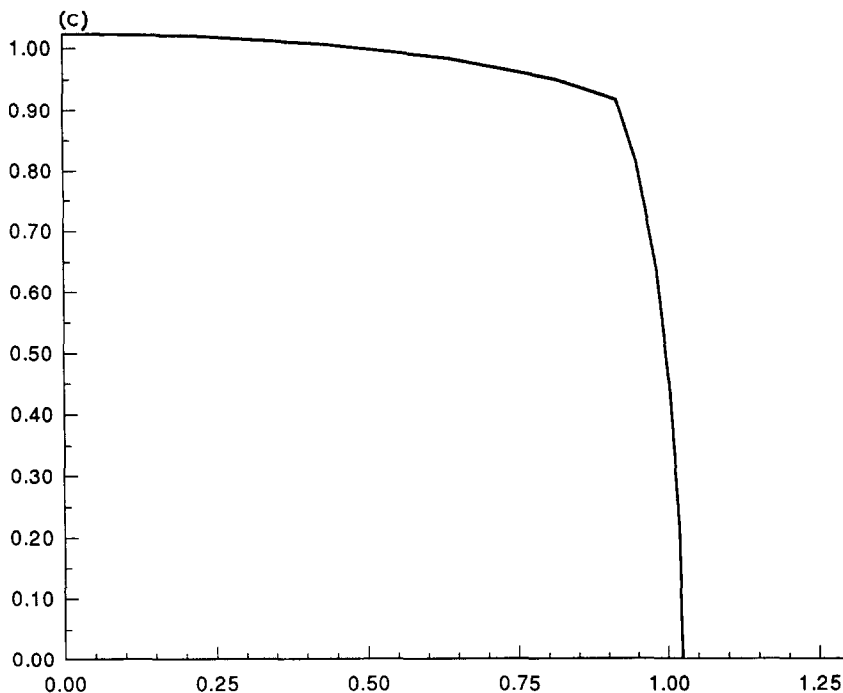


Fig. 11 (continued).

position is measured in radians and is zero in the widest part of the annulus and  $\pi$  in the narrowest part. Three centreline axial velocity traces are presented, two derived from results shown in Fig. 9 (triangles represent Newtonian, squares represent Bingham), and one from the former case where the inner casing is fixed (inverted triangles represent Bingham). Both Bingham materials have a normalised  $Bn$  parameter of 25. When the inner casing rotates about its own axis the limiting Bingham response is a plug flow of constant axial velocity, the extent of which is narrower than the stationary zone created when the inner cylinder remains fixed. The peak axial velocity,  $U_{\max}$ , exists across the widest part of the annulus; to enforce mass flux,  $U_{\max}$  is greatest when the inner cylinder is fixed (owing to the existence of the stationary zone) and the abruptness of the transition zone bridging  $U_{\max}$  to the limiting axial velocity zone is most severe in this instance.

## 7. Conclusion

Good agreement between the numerical predictions and the analytical solutions derived by Walton and Bittleston [21] for the flow of a Bingham

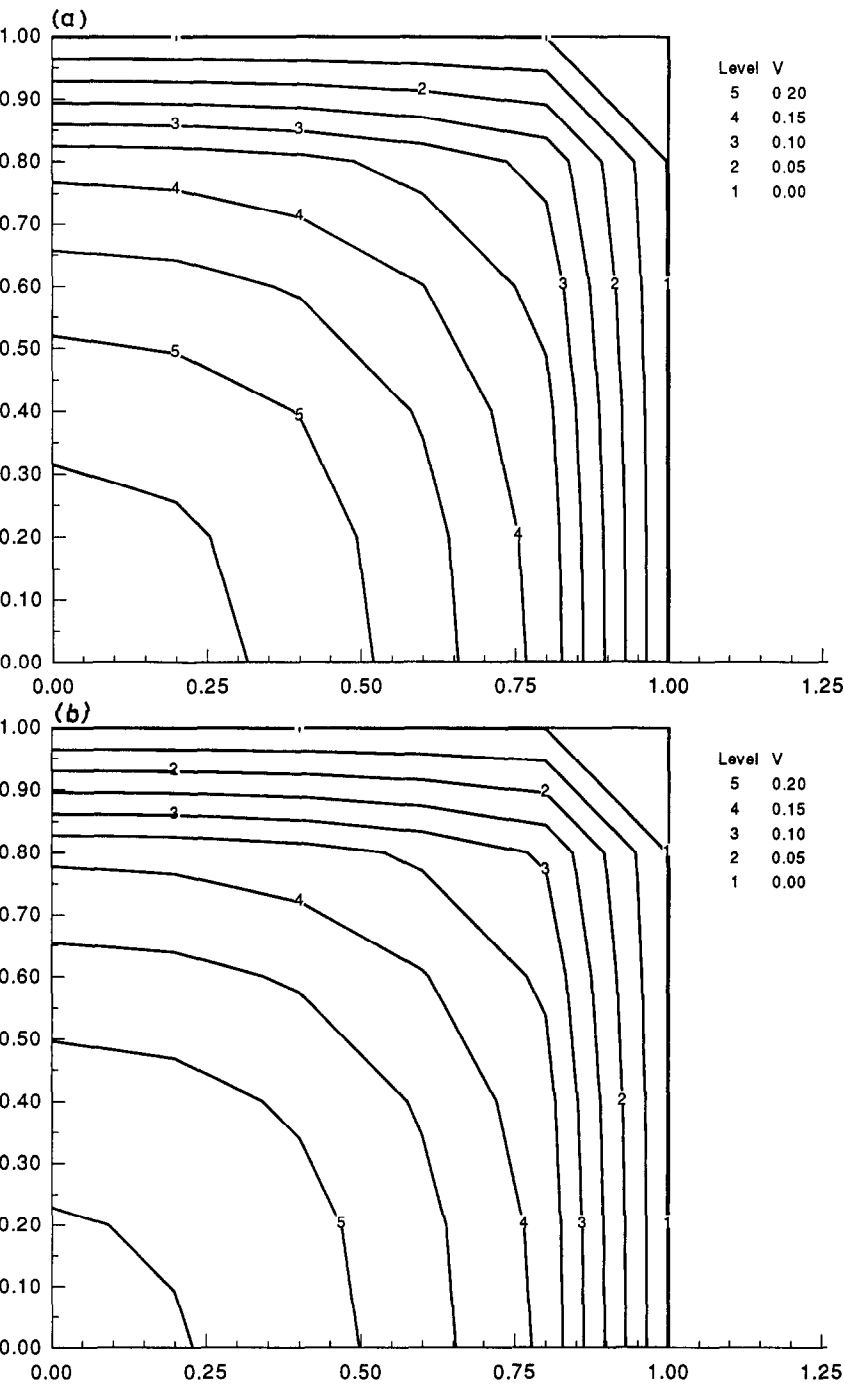


Fig. 12. Axial velocity contours across the die lip for a series of Bingham fluids extruded through a square die. The yield stress is (a)  $\tau_y = 0.05$ ; (b)  $\tau_y = 0.10$ ; (c)  $\tau_y = 0.25$ ; (d)  $\tau_y = 0.50$ ; (e)  $\tau_y = 1.00$ .

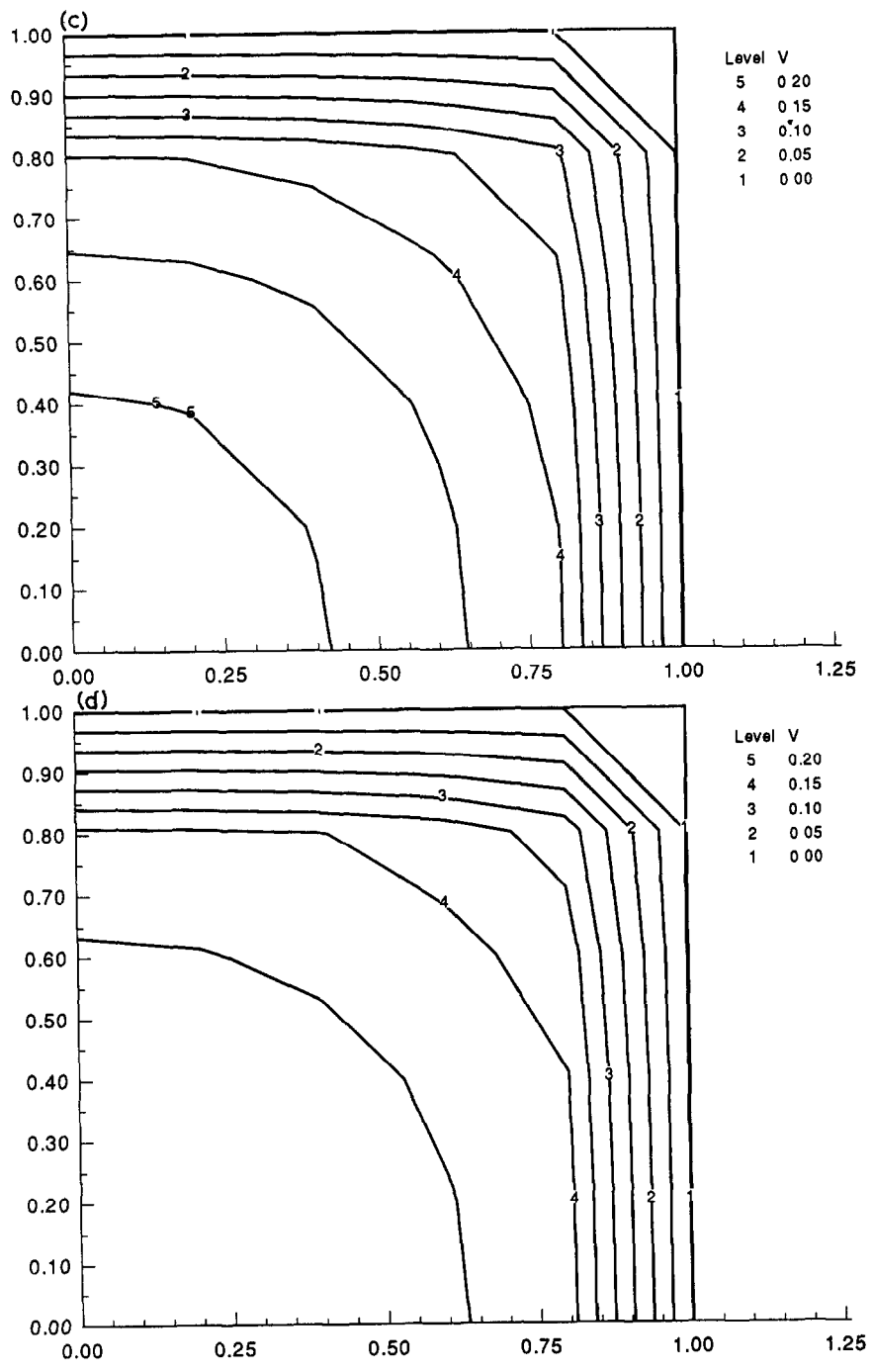


Fig. 12 (continued).

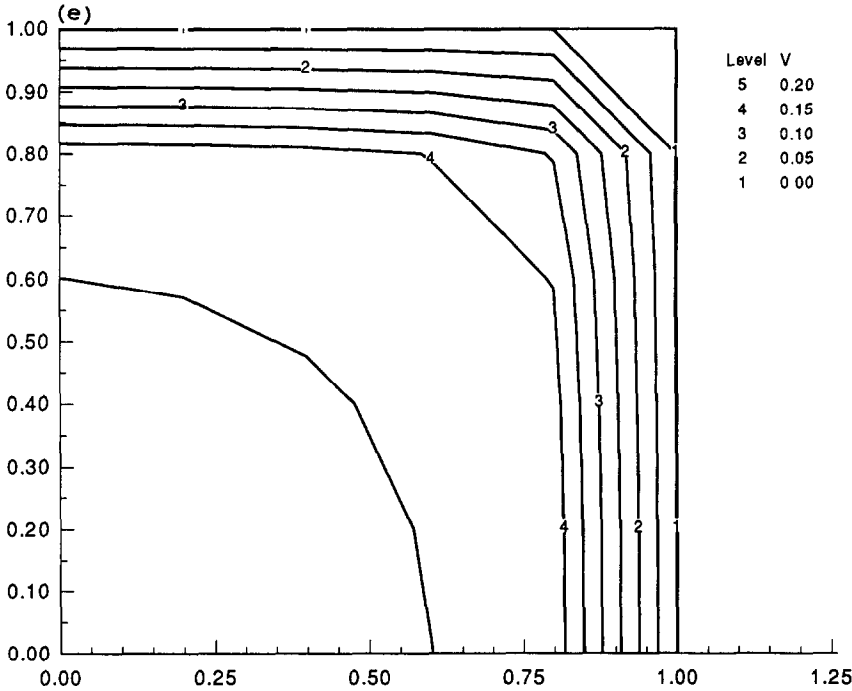


Fig. 12 (continued).

fluid in an eccentric annulus, where the inner casing is fixed, have been obtained. The investigation has been extended to consider the new problem where the inner casing rotates about its own axis with a constant angular velocity.

The examples presented have not been endowed with free surfaces. When considering such problems, define a normalised Bingham number  $Bn$  by

$$Bn = \tau_y \left( \frac{d}{\eta_0 \bar{w}} \right), \quad (31)$$

where  $\bar{w}$  is the average speed,  $\tau_y$  is the yield stress and  $\eta_0$  is a reference viscosity. Consider then a Bingham fluid being forced down a long square tube (side length  $d = 1$ ) and exiting freely at  $x = 4$ . Figure 11 shows the axial velocity contours at  $x = 0$  (inside tube),  $x = 4$  (exit plane) and  $x = 10$  (free body); there is an unyielded zone in the middle of the tube, practically no unyielded zone at exit and the free extrudate which is rigid. In the example shown,  $Bn = 3.58$ . Figure 12 shows the axial velocity contours across the die exit for a series of Bingham materials. Clearly with increasing yield stress the extent of the plug increasingly migrates from the die

TABLE 6

Three-dimensional Bingham square die extrusion extrudate swell ratios assuming no inertia

$\tau_y$	$\chi_A$	$\chi_B$	$U_{\text{plug}}$	$Bn$
0.00	20.507	3.486	0.107	0.000
0.05	15.720	-1.247	0.117	0.358
0.10	12.650	-3.176	0.122	0.717
0.25	6.919	-6.229	0.133	1.792
0.50	2.350	-8.435	0.143	3.584
1.00	-1.481	-10.329	0.151	7.168

Mid-side swelling is denominated by  $\chi_A$ ; corner swelling by  $\chi_B$ .

walls towards the centre of the die. Table 6 summarises the relative extrudate swell ratios defined by

$$\chi = \frac{R_f}{R}, \quad (32)$$

where  $R_f$  is the downstream extrusion half height and  $R$  is the half-die

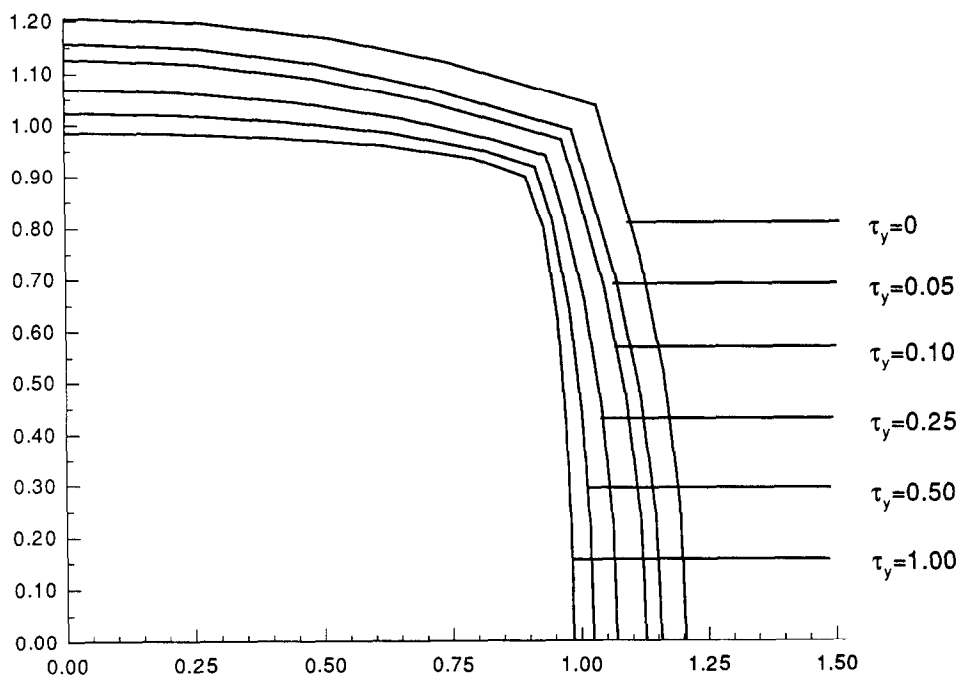


Fig. 13. Downstream cross-sectional extrudate profiles for a series of Bingham fluids extruded through a square die with sides of length unity. With constant mass flux and increasing yield stress ( $\tau_y = 0.0$ ,  $\tau_y = 0.05$ ,  $\tau_y = 0.10$ ,  $\tau_y = 0.25$ ,  $\tau_y = 0.50$  and  $\tau_y = 1.0$ ) the degree of extrudate swell is significantly reduced, as summarised in Table 6.

height, for a series of Bingham materials extruded through a square die. Also shown in the table is the downstream plug flow velocity and normalised Bingham number; Fig. 13 shows the downstream extrudate profiles for the cases included in the table. The Fortin elements have already been shown to perform within acceptable limits of accuracy whilst maintaining a low computational overhead when applied to Newtonian free surface problems [15] and are here proven to be useful three-dimensional incompressible elements capable of solving viscous Bingham extrusion problems.

Finally, the biviscosity model [22] has proved to be a convenient and reliable method of predicting materials with a yield stress, provided one chooses a reference viscosity,  $\eta_r$ , to be three orders of magnitude greater than the imposed yield stress,  $\tau_y$ . The inelastic model described produces features similar to a Bingham response.

## Acknowledgement

This work was supported by the Australian Research Grants Scheme. The support is gratefully acknowledged.

## References

- 1 R.B. Bird, G.C. Dai and B.J. Yarusso, *Rev. Chem. Eng.*, 1 (1984) 1.
- 2 R.I. Tanner, *Engineering Rheology*, revised edn., Oxford University Press, Oxford, 1988.
- 3 J.L. White and H. Tanaka, *J. Non-Newtonian Fluid Mech.*, 8 (1981) 1.
- 4 J.L. White, *J. Non-Newtonian Fluid Mech.*, 8 (1981) 195.
- 5 R. Hill, *The Mathematical Theory of Plasticity*, Oxford University Press, Oxford, 1956.
- 6 A.N. Beris, J.A. Tsamopoulos, R.C. Armstrong and R.A. Brown, *J. Fluid Mech.*, 158 (1985) 219.
- 7 J.F. Milthorpe and R.I. Tanner, *Third Int. Conf. on Numerical Methods in Laminar and Turbulent Flow*, University of Washington, Seattle, 1983.
- 8 E.J. O'Donovan and R.I. Tanner, *J. Non-Newtonian Fluid Mech.*, 15 (1984) 75.
- 9 C.R. Beverly and R.I. Tanner, *J. Rheol.*, 33 (1989) 989.
- 10 K.R.J. Ellwood, G.C. Georgiou, T.C. Papanastasiou and J.O. Wilkes, *J. Rheol.*, 34 (1990) 787.
- 11 T.C. Papanastasiou, *J. Rheol.*, 31 (1987) 385.
- 12 P. Hood and C. Taylor, *Computers and Fluids*, 1 (1973) 73.
- 13 R.E. Nickell, R.I. Tanner and B. Caswell, *J. Fluid Mech.*, 65 (1974) 189.
- 14 O.C. Zienkiewicz, *The Finite Element Method*, 3rd. revised edn., McGraw-Hill Book Company, London, 1977.
- 15 C.R. Beverly and R.I. Tanner, *Rheol. Acta*, 30 (1991) 341.
- 16 M. Fortin, *Int. J. Num. Meth. Fluids*, 1 (1981) 347.
- 17 M. Fortin and A. Fortin, *Int. J. Num. Meth. Fluids*, 5 (1985) 911.
- 18 R.B. Bird, R.C. Armstrong and O. Hassager, *Dynamics of Polymeric Liquids*, Vol. 1, Fluid Mechanics, John Wiley, New York, 1977.
- 19 A.G. Fredrickson and R.B. Bird, *Ind. Eng. Chem.*, 50 (1958) 347.

- 20 J.R.A. Pearson, Xth Int. Congress on Rheology, Sydney University, Sydney, Australia, 1988, 1.73.
- 21 I.C. Walton and S.H. Bittleston, J. Fluid Mech., 222 (1991) 39.
- 22 R.I. Tanner and C.R. Beverly, Proc. Fourth Nat. Congress on Rheology, Flinders University, South Australia, 1986.